

Quantum Chemical Studies on Structural, Spectroscopic, Thermochemistry, Photo-physical and Bioactivity Properties of m-Cresol Purple Dye

Mohamed A.M. El-Mansy ^{1,2}, Athisaya Suvitha ³, Medhat Ibrahim ^{4,*}

¹ Molecular Modeling Simulation Lab., Department of Physics, Faculty of Education, Ain Shams University, Roxy, Cairo, Egypt

² Condensed Matter Theory Group, Department of Physics, College of Science and Arts, Qassim University, Ar Rass, 51921, Saudi Arabia

³ Department of Physics, CMR Institute of Technology, Bangalore, Karnataka, India

⁴ Molecular Spectroscopy and Modeling Unit, Spectroscopy Department, National Research Centre, 33 El-Bohouth St., 12622 Dokki, Giza, Egypt

* Correspondence: ma.khalek@nrc.sci.eg;

Scopus Author ID 8641587100

Received: 15.02.2021; Revised: 5.04.2021; Accepted: 9.04.2021; Published: 26.04.2021

Abstract: The m-Cresol purple molecule is analyzed using spectroscopy and quantum computational chemistry methods using the software program Gaussian 09. B3LYP 6-311G (d, p) level has been used to create stable conformation of molecular structure, vibrational frequencies, Mulliken atomic charges, and electronic absorption spectra. The active regions of the infrared intensities, polarizabilities, and first-order polarizabilities were determined. The visible ultrasonic absorption with DOS spectrum demonstrated the highest correlation both before and after UV exposure. Furthermore, 'Frontier's molecular orbital analysis was determined, explaining the difference between HOMOs and LUMOs energies. Swiss ADME is used to measure physicochemical descriptors and the prediction of molecular dynamics, ADME (absorption, distribution, metabolism, excretion) coefficients, pharmaco-kinetics pH, log P, biological activity, and drug-like nature. Furthermore, the predictive model of BOILED-Egg, QSAR analysis, molecular lipophilicity, distribution of microorganisms, target binding percentages, and topology measurements are analyzed to help drug discovery.

Keywords: band offsets; thermochemistry, nonlinear optics; ADME; QSAR.

© 2021 by the authors. This article is an open-access article distributed under the terms and conditions of the Creative Commons Attribution (CC BY) license (<https://creativecommons.org/licenses/by/4.0/>).

1. Introduction

Worldwide seek urged scientists' core researches to fabricate novel efficient solar cells [1,2]. Recent solar devices are mainly based on organic materials due to affordable fabrication, outstanding potential efficiencies [3, 4], and the ease of photocurrent enhancement upon tailoring their molecular structure [5,6]. Meta-cresol purple (m-CP) has been used in seawater pH column assessments in various ocean zones [7,8]. Seawater pH characterizes the ocean's acid-based framework upon certain equilibrium circumstances (salinity, temperature, pressure) [9]. pH values index the oceanic CO₂ system, reflecting major procedures like production and respiration, air-sea CO₂ exchange, and CaCO₃ dissolution. m-CP has a chemical formula C₂₁H₁₈O₅S and its molecular mass is 382.0875 a.m.u, as shown in Fig.1-a. The Molecular simulation technique recently turned into a unique tool to foresee both structural, spectral, and thermochemical features through computational-based programs. Authors used molecular simulation as significant spectroscopic confirmation means for their experimental FT-IR

spectra [10]. Density functional principles (DFT) using Becke's three functionals with Lee, Yang & Parr (B3LYP) selecting 6-311G level is an excellent well-known fashion for computing FTIR spectra [11-19] as well as complex heteromoties bonding and conducting polymers optoelectronic aspects [14] whereas WB97XD6-311G level is used for nonlinear optics (NLO) calculations.

As recently reported, m-CP structural, electronic, optical, and nonlinear optical (NLO) properties have not been published yet. Accordingly, such a study will be a step towards investigating m-CP characteristics in advance.

2. Materials and Methods

2.1. Computational details.

A theoretical approach is carried out through collaborated Gaussian (G09) [20] with Gauss View 5 (GV5) [21] software considering the B3LYP6-311G set. m-CP optimum geometry, FTIR charts, HOMO~LUMO bandgap, ionized-potential IP, electron-affinity EA, chemical-potential χ , hardness κ , electrophile-index ϕ , softness S are computed by the same trend. Also, m-CP NLO response is checked using the WB97XD6-311G set. The density of state charts is resolved through Gauss Sum 3. Drug bank computation carried out the QSAR study, the molecular lipophilicity of m-CP [22-24]. ADME parameters, pharmacophore modeling, pharmaco-kinetics / pharmaco-dynamics, metabolism, Boiled-Egg predictive model, biological activity radar, and target binding percentage were performed using Swiss ADME software [25-27]. The distribution of microorganisms and topology measurements are also determined by the Marvin sketch program [28-30] to analyze the active region of the compound.

3. Results and Discussion

3.1. Optimum geometry.

Computed B3LYP6-311G crystallographic parameters for m-CP are registered in Table 1. Inasmuch as crystallographic data paucity on m-CP, experimental/theoretical crystal report will not be registered in the meantime. According to optimal m-CP geometry (see Fig.1-b), remarkable weak interactions have been observed between OH group attached to SO₂ with adjacent Phenol moiety. 2 virtual bonds C₂₂-O₃₃, C₂₃-O₃₁ of 4.48, 3.12 Å, and 9 virtual angles C₂₁-C₂₂-O₃₃, C₂₄-C₂₂-O₃₃, O₃₃-C₂₂-C₃₅, C₂₁-C₂₃-O₃₁, C₂₅-C₂₃-O₃₁, C₂₆-C₂₃-O₃₁, C₂₃-O₃₁-S₃₀, C₂₂-O₃₃-S₃₀, C₂₂-O₃₃-H₃₄ of 69.01°, 88.54°, 113.80°, 87.71°, 124.31°, 55.46°, 97.45°, 100.56°, 59.85°, respectively, registered in Table 1 (see red highlights). Also, 26 virtual torsion angles are registered in Table 1 due to twisted SO₃H-phenol interactions (see red highlights). Such interactions are expected to impact both electronic and photovoltaic properties of m-CP highly.

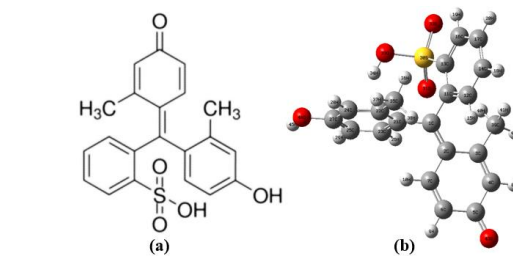


Figure 1. (a) Chemical; (b) Optimum scheme for m-CP.

Table 1. Calculated m-CP crystal coefficients.

bond-extent	(Å)	torsion-angle	(°)
C ₁ -C ₂	1.39	C ₁₁ -C ₁ -C ₂ -C ₃	-24.75
C ₁ -C ₁₁	1.50	C ₁₁ -C ₁ -C ₂ -C ₇	155.13
C ₁ -C ₂₁	1.50	C ₂₁ -C ₁ -C ₂ -C ₃	158.47
C ₂ -C ₃	1.49	C ₂₁ -C ₁ -C ₂ -C ₇	-21.65
C ₂ -C ₇	1.47	C ₂ -C ₁ -C ₁₁ -C ₁₂	-56.84
C ₃ -C ₄	1.37	C ₂ -C ₁ -C ₁₁ -C ₁₃	127.27
C ₃ -C ₃₉	1.52	C ₂₁ -C ₁ -C ₁₁ -C ₁₂	120.05
C ₄ -C ₅	1.47	C ₂₁ -C ₁ -C ₁₁ -C ₁₃	-55.83
C ₄ -H ₈	1.09	C ₂ -C ₁ -C ₂₁ -C ₂₂	125.50
C ₅ -C ₆	1.47	C ₂ -C ₁ -C ₂₁ -C ₂₃	-55.59
C ₅ -O ₄₃	1.27	C ₁₁ -C ₁ -C ₂₁ -C ₂₂	-51.43
C ₆ -C ₇	1.36	C ₁₁ -C ₁ -C ₂₁ -C ₂₃	127.48
C ₆ -H ₉	1.09	C ₁ -C ₂ -C ₃ -C ₄	173.92
C ₇ -H ₁₀	1.09	C ₁ -C ₂ -C ₃ -C ₃₉	-13.96
C ₁₁ -C ₁₂	1.42	C ₇ -C ₂ -C ₃ -C ₄	-5.96
C ₁₁ -C ₁₃	1.41	C ₇ -C ₂ -C ₃ -C ₃₉	166.16
C ₁₂ -C ₁₄	1.40	C ₁ -C ₂ -C ₇ -C ₆	-172.31
C ₁₂ -H ₁₅	1.09	C ₁ -C ₂ -C ₇ -H ₁₀	2.46
C ₁₃ -C ₁₆	1.40	C ₃ -C ₂ -C ₇ -C ₆	7.58
C ₁₃ -S ₃₀	1.88	C ₃ -C ₂ -C ₇ -H ₁₀	-177.65
C ₁₄ -C ₁₇	1.41	C ₂ -C ₃ -C ₄ -C ₅	-0.02
C ₁₄ -H ₁₈	1.09	C ₂ -C ₃ -C ₄ -H ₈	176.98
C ₁₆ -C ₁₇	1.41	C ₃₉ -C ₃ -C ₄ -C ₅	-172.45
C ₁₆ -H ₁₉	1.09	C ₃₉ -C ₃ -C ₄ -H ₈	4.55
C ₁₇ -H ₂₀	1.09	C ₂ -C ₃ -C ₃₉ -C ₄₀	-43.22
C ₂₁ -C ₂₂	1.43	C ₂ -C ₃ -C ₃₉ -H ₄₁	78.05
C ₂₁ -C ₂₃	1.42	C ₂ -C ₃ -C ₃₉ -H ₄₂	-162.02
C ₂₂ -C ₂₄	1.41	C ₄ -C ₃ -C ₃₉ -H ₄₀	128.96
C ₂₂ -O ₃₃	3.48	C ₄ -C ₃ -C ₃₉ -H ₄₁	-109.78
C ₂₂ -C ₃₅	1.52	C ₄ -C ₃ -C ₃₉ -H ₄₂	10.16
C ₂₃ -C ₂₅	1.40	C ₃ -C ₄ -C ₅ -C ₆	4.74
C ₂₃ -H ₂₆	1.08	C ₃ -C ₄ -C ₅ -O ₄₃	-176.55
C ₂₃ -O ₃₁	3.12	H ₈ -C ₄ -C ₅ -C ₆	-172.40
C ₂₄ -C ₂₇	1.41	H ₈ -C ₄ -C ₅ -O ₄₃	6.31
C ₂₄ -H ₂₈	1.09	O ₃₃ -C ₂₂ -C ₃₅ -H ₃₆	-4.30
C ₂₅ -C ₂₇	1.41	O ₃₃ -C ₂₂ -C ₃₅ -H ₃₇	115.28
C ₂₅ -H ₂₉	1.09	O ₃₃ -C ₂₂ -C ₃₅ -H ₃₈	-124.47
C ₂₇ -O ₄₄	1.09	C ₂₁ -C ₂₃ -C ₂₅ -C ₂₇	-1.30
S ₃₀ -O ₃₁	1.61	C ₂₁ -C ₂₃ -C ₂₅ -H ₂₉	179.29
S ₃₀ -O ₃₂	1.60	H ₂₆ -C ₂₃ -C ₂₅ -C ₂₇	-178.70
S ₃₀ -O ₃₃	1.80	H ₂₉ -C ₂₅ -C ₂₇ -C ₂₄	179.68
O ₃₃ -H ₃₄	0.99	H ₂₉ -C ₂₅ -C ₂₇ -O ₄₄	0.06
C ₃₅ -H ₃₆	1.10	C ₂₄ -C ₂₇ -O ₄₄ -H ₄₅	-179.30
C ₃₅ -H ₃₇	1.10	C ₂₅ -C ₂₇ -O ₄₄ -H ₄₅	0.34
C ₃₅ -H ₃₈	1.10	O ₃₂ -S ₃₀ -O ₃₃ -H ₃₄	145.61
C ₃₉ -H ₄₀	1.10	C ₄ -C ₅ -C ₆ -C ₇	-3.23
C ₃₉ -H ₄₁	1.09	C ₄ -C ₅ -C ₆ -H ₉	178.31
C ₃₉ -H ₄₂	1.09	O ₄₃ -C ₅ -C ₆ -C ₇	178.06
O ₄₄ -H ₄₅	0.98	O ₄₃ -C ₅ -C ₆ -H ₉	-0.40
C ₂ -C ₁ -C ₁₁	122.04	C ₅ -C ₆ -C ₇ -C ₂	-2.90
C ₂ -C ₁ -C ₂₁	120.83	C ₅ -C ₆ -C ₇ -H ₁₀	-177.56
C ₁₁ -C ₁ -C ₂₁	117.03	H ₉ -C ₆ -C ₇ -C ₂	175.48
C ₁ -C ₂ -C ₃	125.11	H ₉ -C ₆ -C ₇ -H ₁₀	0.82
C ₁ -C ₂ -C ₇	118.26	C ₁ -C ₁₁ -C ₁₂ -C ₁₄	-175.00
C ₃ -C ₂ -C ₇	116.63	C ₁ -C ₁₁ -C ₁₂ -H ₁₅	3.69
C ₂ -C ₃ -C ₄	119.00	C ₁₃ -C ₁₁ -C ₁₂ -C ₁₄	1.35
C ₂ -C ₃ -C ₃₉	122.21	C ₁₃ -C ₁₁ -C ₁₂ -H ₁₅	-179.95
C ₄ -C ₃ -C ₃₉	118.34	C ₁ -C ₁₁ -C ₁₃ -C ₁₆	174.61
C ₃ -C ₄ -C ₅	124.10	C ₁ -C ₁₁ -C ₁₃ -S ₃₀	-12.33
C ₃ -C ₄ -H ₈	120.49	C ₁₂ -C ₁₁ -C ₁₃ -C ₁₆	-1.37
C ₅ -C ₄ -H ₈	115.35	C ₁₂ -C ₁₁ -C ₁₃ -S ₃₀	171.69
C ₄ -C ₅ -C ₆	115.88	C ₁₁ -C ₁₂ -C ₁₄ -C ₁₇	-0.14
C ₄ -C ₅ -O ₄₃	121.90	C ₁₁ -C ₁₂ -C ₁₄ -H ₁₈	179.71
C ₆ -C ₅ -O ₄₃	122.20	H ₁₅ -C ₁₂ -C ₁₄ -C ₁₇	-178.81
C ₅ -C ₆ -C ₇	120.85	H ₁₅ -C ₁₂ -C ₁₄ -H ₁₈	1.04

bond-extent	(Å)	torsion-angle	(°)
C ₅ -C ₆ -H ₉	117.14	H ₁₁ -C ₁₃ -C ₁₆ -C ₁₇	0.14
C ₇ -C ₆ -H ₉	121.99	H ₁₁ -C ₁₃ -C ₁₆ -H ₁₉	178.12
C ₂ -C ₇ -C ₆	122.97	S ₃₀ -C ₁₃ -C ₁₆ -C ₁₇	-173.45
C ₂ -C ₇ -H ₁₀	117.42	S ₃₀ -C ₁₃ -C ₁₆ -H ₁₉	4.54
C ₆ -C ₇ -H ₁₀	119.42	C ₁₁ -C ₁₃ -S ₃₀ -O ₃₁	-30.28
C ₁ -C ₁₁ -C ₁₂	117.75	C ₁₁ -C ₁₃ -S ₃₀ -O ₃₂	-163.21
C ₁ -C ₁₁ -C ₁₃	126.91	C ₁₁ -C ₁₃ -S ₃₀ -O ₃₃	86.29
C ₁₂ -C ₁₁ -C ₁₃	115.22	C ₁₆ -C ₁₃ -S ₃₀ -O ₃₁	143.47
C ₁₁ -C ₁₂ -C ₁₄	122.09	C ₁₆ -C ₁₃ -S ₃₀ -O ₃₂	10.54
C ₁₁ -C ₁₂ -C ₁₅	118.00	C ₁₆ -C ₁₃ -S ₃₀ -O ₃₃	-99.96
C ₁₄ -C ₁₂ -C ₁₅	119.90	C ₁₂ -C ₁₄ -C ₁₇ -C ₁₆	-1.17
C ₁₁ -C ₁₃ -C ₁₆	124.21	C ₁₂ -C ₁₄ -C ₁₇ -H ₂₀	179.76
C ₁₁ -C ₁₃ -S ₃₀	122.06	H ₁₈ -C ₁₄ -C ₁₇ -C ₁₆	178.98
C ₁₆ -C ₁₃ -S ₃₀	113.41	H ₁₈ -C ₁₄ -C ₁₇ -H ₂₀	-0.09
C ₁₂ -C ₁₄ -C ₁₇	120.42	H ₂₆ -C ₂₃ -C ₂₅ -H ₂₉	1.89
C ₁₂ -C ₁₄ -C ₁₈	119.50	O ₃₁ -C ₂₃ -C ₂₅ -C ₂₇	-112.17
C ₁₇ -C ₁₄ -C ₁₈	120.08	O ₃₁ -C ₂₃ -C ₂₅ -H ₂₉	68.43
C ₁₃ -C ₁₆ -C ₁₇	118.72	C ₂₁ -C ₂₃ -O ₃₁ -S ₃₀	-47.29
C ₁₃ -C ₁₆ -H ₁₉	119.82	C ₂₅ -C ₂₃ -O ₃₁ -S ₃₀	80.21
C ₁₇ -C ₁₆ -H ₁₉	121.43	H ₂₆ -C ₂₃ -O ₃₁ -S ₃₀	-175.10
C ₁₄ -C ₁₇ -C ₁₆	119.32	C ₁₃ -S ₃₀ -O ₃₁ -C ₂₃	74.02
C ₁₄ -C ₁₇ -H ₂₀	120.78	O ₃₂ -S ₃₀ -O ₃₁ -C ₂₃	-159.91
C ₁₆ -C ₁₇ -H ₂₀	119.89	O ₃₃ -S ₃₀ -O ₃₁ -C ₂₃	-39.44
C ₁ -C ₂₁ -C ₂₂	123.86	C ₁₃ -S ₃₀ -O ₃₁ -C ₂₂	-41.42
C ₁ -C ₂₁ -C ₂₃	116.99	C ₁₃ -C ₁₆ -C ₁₇ -C ₁₄	1.16
C ₂₂ -C ₂₁ -C ₂₃	119.14	C ₁₃ -C ₁₆ -C ₁₇ -H ₂₀	-179.76
C ₂₁ -C ₂₂ -C ₂₄	118.49	H ₁₉ -C ₁₆ -C ₁₇ -C ₁₄	-176.79
C ₂₁ -C ₂₂ -O ₃₃	69.01	H ₁₉ -C ₁₆ -C ₁₇ -H ₂₀	2.29
C ₂₁ -C ₂₂ -C ₃₅	122.93	C ₁ -C ₂₁ -C ₂₂ -C ₂₄	178.52
C ₂₄ -C ₂₂ -O ₃₃	88.54	C ₁ -C ₂₁ -C ₂₂ -O ₃₃	101.34
C ₂₄ -C ₂₂ -C ₃₅	118.56	C ₁ -C ₂₁ -C ₂₂ -C ₃₅	-3.35
O ₃₃ -C ₂₂ -C ₃₅	113.80	C ₂₃ -C ₂₁ -C ₂₂ -C ₂₄	-0.38
C ₂₁ -C ₂₃ -C ₂₅	121.45	C ₂₃ -C ₂₁ -C ₂₂ -O ₃₃	-77.56
C ₂₁ -C ₂₃ -C ₂₆	118.55	C ₂₃ -C ₂₁ -C ₂₂ -C ₃₅	177.76
C ₂₁ -C ₂₃ -O ₃₁	87.71	C ₁ -C ₂₁ -C ₂₃ -C ₂₅	-177.62
C ₂₅ -C ₂₃ -C ₂₆	119.96	C ₁ -C ₂₁ -C ₂₃ -H ₂₆	-0.20
C ₂₅ -C ₂₃ -O ₃₁	124.31	C ₁ -C ₂₁ -C ₂₃ -O ₃₁	-48.23
C ₂₆ -C ₂₃ -O ₃₁	55.46	C ₂₂ -C ₂₁ -C ₂₃ -C ₂₅	1.35
C ₂₂ -C ₂₄ -C ₂₇	121.95	C ₂₂ -C ₂₁ -C ₂₃ -H ₂₆	178.78
C ₂₂ -C ₂₄ -C ₂₈	118.72	C ₂₂ -C ₂₁ -C ₂₃ -O ₃₁	130.74
C ₂₇ -C ₂₄ -C ₂₈	119.33	C ₂₁ -C ₂₂ -C ₂₄ -C ₂₇	-0.61
C ₂₃ -C ₂₅ -C ₂₇	119.42	C ₂₁ -C ₂₂ -C ₂₄ -H ₂₈	179.07
C ₂₃ -C ₂₅ -H ₂₉	119.95	O ₃₃ -C ₂₂ -C ₂₄ -C ₂₇	65.24
C ₂₇ -C ₂₅ -H ₂₉	120.64	O ₃₃ -C ₂₂ -C ₂₄ -H ₂₈	-115.08
C ₂₄ -C ₂₇ -C ₂₅	119.54	C ₃₅ -C ₂₂ -C ₂₄ -C ₂₇	-178.83
C ₂₄ -C ₂₇ -O ₄₄	120.05	C ₃₅ -C ₂₂ -C ₂₄ -H ₂₈	0.85
C ₂₅ -C ₂₇ -O ₄₄	120.41	C ₂₁ -C ₂₂ -O ₃₃ -S ₃₀	-40.03
C ₁₃ -S ₃₀ -O ₃₁	110.10	C ₂₁ -C ₂₂ -O ₃₃ -H ₃₄	66.12
C ₁₃ -S ₃₀ -O ₃₂	107.56	C ₂₄ -C ₂₂ -O ₃₃ -S ₃₀	-161.55
C ₁₃ -S ₃₀ -O ₃₃	103.80	C ₂₄ -C ₂₂ -O ₃₃ -H ₃₄	-55.41
O ₃₁ -S ₃₀ -O ₃₂	120.35	C ₃₅ -C ₂₂ -O ₃₃ -S ₃₀	77.92
O ₃₁ -S ₃₀ -O ₃₃	109.09	C ₃₅ -C ₂₂ -O ₃₃ -H ₃₄	-175.94
O ₃₂ -S ₃₀ -O ₃₃	104.62	C ₂₁ -C ₂₂ -C ₃₅ -H ₃₆	75.18
C ₂₃ -O ₃₁ -S ₃₀	97.45	C ₂₁ -C ₂₂ -C ₃₅ -H ₃₇	-165.24
C ₂₂ -O ₃₃ -S ₃₀	100.56	C ₂₁ -C ₂₂ -C ₃₅ -H ₃₈	-44.99
C ₂₂ -O ₃₃ -H ₃₄	59.85	C ₂₄ -C ₂₂ -C ₃₅ -H ₃₆	-106.67
S ₃₀ -O ₃₃ -H ₃₄	109.38	C ₂₄ -C ₂₂ -C ₃₅ -H ₃₇	12.91
C ₂₂ -C ₃₅ -H ₃₆	111.65	C ₂₄ -C ₂₂ -C ₃₅ -H ₃₈	133.16
C ₂₂ -C ₃₅ -H ₃₇	110.45	C ₂₂ -C ₂₄ -C ₂₇ -C ₂₅	0.67
C ₂₂ -C ₃₅ -H ₃₈	111.86	C ₂₂ -C ₂₄ -C ₂₇ -O ₄₄	-179.68
H ₃₆ -C ₃₅ -H ₃₇	107.47	H ₂₈ -C ₂₄ -C ₂₇ -C ₂₅	-179.01
H ₃₆ -C ₃₅ -H ₃₈	107.37	H ₂₈ -C ₂₄ -C ₂₇ -O ₄₄	0.63
H ₃₇ -C ₃₅ -H ₃₈	107.84	C ₂₃ -C ₂₅ -C ₂₇ -C ₂₄	0.28
C ₃ -C ₃₉ -H ₄₀	110.69	C ₂₃ -C ₂₅ -C ₂₇ -O ₄₄	-179.35
C ₃ -C ₃₉ -H ₄₁	113.18	C ₁₃ -S ₃₀ -O ₃₃ -H ₃₄	-101.68
C ₃ -C ₃₉ -H ₄₂	109.51	O ₃₁ -S ₃₀ -O ₃₃ -C ₂₂	76.12

bond-extent	(Å)	torsion-angle	(°)
H ₄₀ -C ₃₉ -H ₄₁	107.91	O ₃₁ -S ₃₀ -O ₃₃ -H ₃₄	15.86
H ₄₀ -C ₃₉ -H ₄₂	107.85	O ₃₂ -S ₃₀ -O ₃₃ -C ₂₂	-154.13
H ₄₁ -C ₃₉ -H ₄₂	107.52		
C ₂₇ -O ₄₄ -H ₄₅	107.95		

3.2. FTIR analyses.

For convenience, authors select only 27 modes among 129 others to concur with recorded m-CP FTIR wavenumbers assigned in Table 2. Assignments are performed through GV 5, considering that the predicted wavenumber is a scale of 0.96 [31] to fit with experimental data. A proper harmony between measured and predicted FTIR charts is noticed. Fig. 2 shows both measured and computed FTIR charts. m-CP assignments are briefly discussed as:

3.2.1. Single-bond vibrations.

OH stretch is detected between 3400 - 3500 cm⁻¹[32]. Mode 1 is assigned to OH stretch at 3409cm⁻¹, comparable to experimental at 3450 cm⁻¹. Mode 12 is attributed to OH scissoring at 1243cm⁻¹, commensurate to an observed band at 1246 cm⁻¹. Modes (18, 19) are referred to OH wagging and twisting at 884, 852 cm⁻¹, balanced to recorded bands at 885, 850 cm⁻¹, respectively.

CH stretch is perceived among 3300–3000 cm⁻¹ [33]. Modes (2, 3) are imputed to both asymmetric and symmetric terminal CH stretch at 3116, 3114 cm⁻¹, corresponding to experimental ones at 3242, 3160 cm⁻¹. Modes (4, 5) are referred to as both non-symmetric and symmetric ring CH stretch at 3100, 3085 cm⁻¹, analogous to recorded bands at 3100, 3050 cm⁻¹. Modes (13-15) are specified for CH scissoring and rocking at 1226, 1131, 1068cm⁻¹, proportionate to measured values at 1215, 1122, 1083 cm⁻¹, respectively. Modes (19-22) are related to CH wagging and twisting at 852, 795, 765, 729 cm⁻¹, analogous to recognized peaks at 850, 772, 760, 723 cm⁻¹, respectively. Modes (10, 11) are mentioned to CH₃ deformations at 1470, 1434 cm⁻¹, analogous to indexed data at 1467, 1433 cm⁻¹.

Mode 16 is attributed to SO+SC stretch at 1025 cm⁻¹, analogous to defined peak at 1016 cm⁻¹ [34]. Mode 17 is allocated to CO+CC stretch at 996cm⁻¹, comparable to the observed value at 960 cm⁻¹. Mode 23 is specified for SO+SC+CO+ CC scissoring at 671cm⁻¹, corresponding to index measure at 666 cm⁻¹. Mode 24 is verified for SO+SC+CO+CC wagging at 567 cm⁻¹, comparative to the recorded pattern at 556 cm⁻¹.

3.2.2. Double-bond vibrations.

C=O, as well as C=C stretch, is noticed amidst 1750-1500 cm⁻¹ [35]. Mode 6 is approved for C=O stretch at 1612cm⁻¹, correspond to the observed value at 1613 cm⁻¹. Modes (7-9) are referred to C=C stretch at 1593, 1542, 1540 cm⁻¹, concur to experimental data at 1583, 1552, 1506 cm⁻¹.

3.3. Mulliken distribution analyses.

A direct way to describe molecule electronic properties such as free carriers transport or electro negatively can be easily achieved through Mulliken distribution of charges [36]. Mulliken distributions of m-CP partial charges (Q) are registered in Table 3. Distribution of Mulliken m-CP partial charges present in Fig. 3. Positive Q-values are allocated on C₁, C₂, C₃,

C₅, C₁₀, C₁₁, C₂₁, C₂₂, and all H atoms, while negative Q-values are set on others. Unusual electrostatic interactions are observed between O₃₃ with both C₂₂ and C₂₃, which are expected to impact NLO behavior of m-CP.

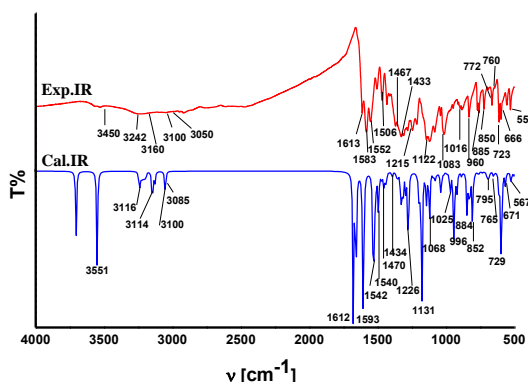


Figure 2. Observed and calculated FTIR charts for m-CP.

Table 2. Recorded and theoretical FTIR wavenumbers, IR intensities and corresponding assignments for m-CP.

No	Exp. (cm ⁻¹)	Cal. (cm ⁻¹)		IR		Vibrational assignments
		Non-scaled	Scaled	Rel.	Abs.	
1	3450	3551	3409	127	60	v OH
2	3242	3246	3116	0	0	v _{as} CH (CH ₃)
3	3160	3244	3114	15	7	v _s CH (CH ₃)
4	3100	3229	3100	6	3	v _{as} CH (Ring)
5	3050	3214	3085	10	5	v _s CH (Ring)
6	1613	1679	1612	200	94	v C=O
7	1583	1659	1593	171	80	
8	1552	1606	1542	109	51	
9	1506	1604	1540	124	58	
10	1467	1531	1470	119	56	
11	1433	1494	1434	57	27	CH ₃ deformations
12	1246	1295	1243	24	11	ζ OH
13	1215	1277	1226	107	50	ζ CH
14	1122	1178	1131	213	100	ζ CH
15	1083	1112	1068	45	21	ρ CH
16	1016	1068	1025	5	2	v SO+SC
17	960	1037	996	35	16	v CO+CC
18	885	921	884	20	9	τ OH
19	850	887	852	6	3	ω OH
20	772	828	795	128	60	τ CH
21	760	797	765	10	5	τ CH
22	723	759	729	2	1	ω CH
23	666	699	671	14	7	ζ SO+SC+CO+CC
24	556	591	567	35	16	ω SO+SC+CO+CC

v (stretch); v_s(symmetric); v_{as}(non – symmetric); ζ(scissoring); ρ(rocking); ω (wagging); τ(twisting)

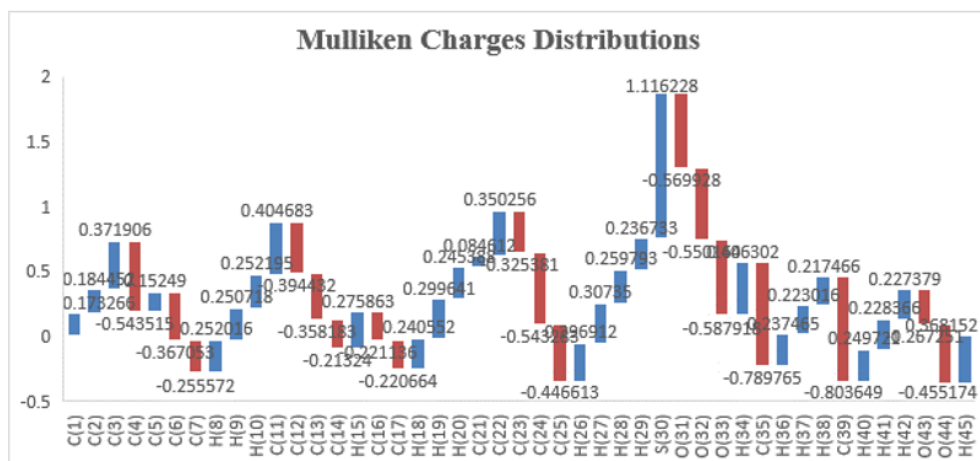


Figure 3. Mulliken distributions for m-CP charges.

Table 3. Mulliken distributions for m-CP charges.

Atom	Q (a.u)	Atom	Q (a.u)
C ₁	0.173266	C ₂₄	-0.543283
C ₂	0.184452	C ₂₅	-0.446613
C ₃	0.371906	H ₂₆	0.296912
C ₄	-0.543515	H ₂₇	0.30735
C ₅	0.15249	H ₂₈	0.259793
C ₆	-0.367053	H ₂₉	0.236733
C ₇	-0.255572	S ₃₀	1.116228
H ₈	0.252016	O ₃₁	-0.569928
H ₉	0.250718	O ₃₂	-0.550164
H ₁₀	0.252195	O ₃₃	-0.587918
C ₁₁	0.404683	H ₃₄	0.406302
C ₁₂	-0.394432	C ₃₅	-0.789765
C ₁₃	-0.358183	H ₃₆	0.237465
C ₁₄	-0.21324	H ₃₇	0.223016
H ₁₅	0.275863	H ₃₈	0.217466
C ₁₆	-0.221136	C ₃₉	-0.803649
C ₁₇	-0.220664	H ₄₀	0.249721
H ₁₈	0.240552	H ₄₁	0.228366
H ₁₉	0.299641	H ₄₂	0.227379
H ₂₀	0.245388	O ₄₃	-0.267251
C ₂₁	0.084612	O ₄₄	-0.455174
C ₂₂	0.350256	H ₄₅	0.368152
C ₂₃	-0.325381		

3.4. Thermo-chemistry and frontier molecular orbital (FMOs) analyses.

Thermo-dynamical parameters like total-energy (TE), absolute zero-energy (AZE), rotation-coefficients (RCs), entropy (S), specific-heat (C_v), overall dipole-moment (TDM), nuclear repulsive-potential (NRP), and HOMO~LUMO offset for m-CP are calculated and listed in Table 4.

Table 4 Thermo-chemistry, E_{LUMO}, E_{HOMO} and E_{LUMO/HOMO} offset for m-CP before and after UV exposure.

Parameters	Before UV	After UV
TE(Hartree)	-1584.96253	-1583.70425
AZE(Kcal/Mol)	215.35014	201.52769
RCs(GHz)	0.21044 0.16587 0.12202	0.21625 0.18408 0.12481
S(Cal/Mol·°K)		
Total	168.1	161.149
Transational	43.714	43.698
Vibrational	35.577	35.424
Rotational	88.809	82.027
C _v (Cal/Mol·°K)		
Total	96.61	92.102
Transational	2.981	2.981
Vibrational	2.981	2.981
Rotational	90.648	86.141
NRP(eV)	7.7*10 ⁴	7.2*10 ⁴
TDM(Debye)	5.72	8.99
E _{LUMO} (eV)	-3.06	-4.14
E _{HOMO} (eV)	-6.80	-6.80
E _{LUMO/HOMO} (eV)	3.75	2.66
IP(eV)	3.06	0.15
EA(eV)	6.80	0.25
χ (eV)	1.87	1.33
κ (eV)	-4.93	-5.47
ϕ (eV)	6.49	11.27
S (eV ⁻¹)	0.53	0.75

Quantum-chemistry researchers apply FMOs analyses to expect reactivities as well as to justify reaction-pathway mechanisms [37]. Reaction pathways, as well as reactivity, are

related to how intensive HOMOs/LUMOs interactions are. Outstanding physical features are derived such interactions like ionized-potential $IP = -E_{HOMO}$, electron-affinity $EA = -E_{LUMO}$, chemical-potential $\chi = (E_{LUMO} + E_{HOMO})/2$, hardness $\kappa = (E_{LUMO} - E_{HOMO})/2$, electrophile-index $\phi = \chi^2/2\kappa$ and softness $S = 1/\kappa^{24}$. m-CP molecule has a high dipole-moment (5.72 D) and HOMO/LUMO offset of 3.75 eV (see Fig.4(a)) which may compete Si & Ge based-solar cells band offsets (3.9and 2.8 eV, respectively) [25]. Such evidence stimulates researchers' insights to fabricate new m-CP based solar devices and check their efficiencies. Fig. 5-a presents the calculated DOS chart for m-CP.

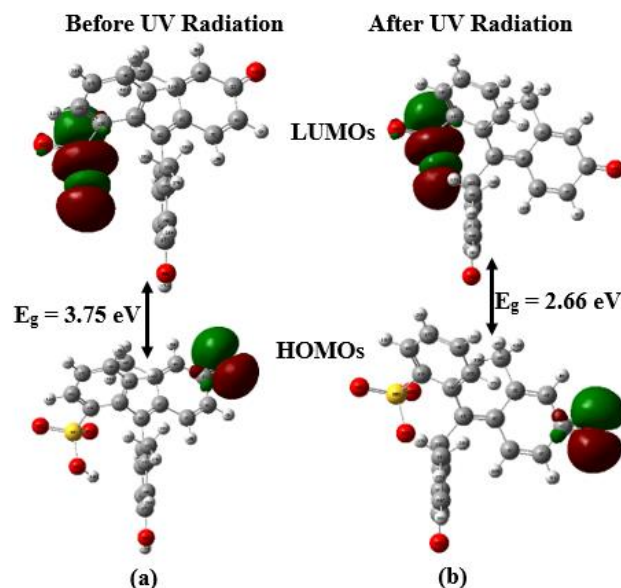


Figure 4. HOMO/LUMO offsets for m-CP (a) before, (b) after UV exposure.

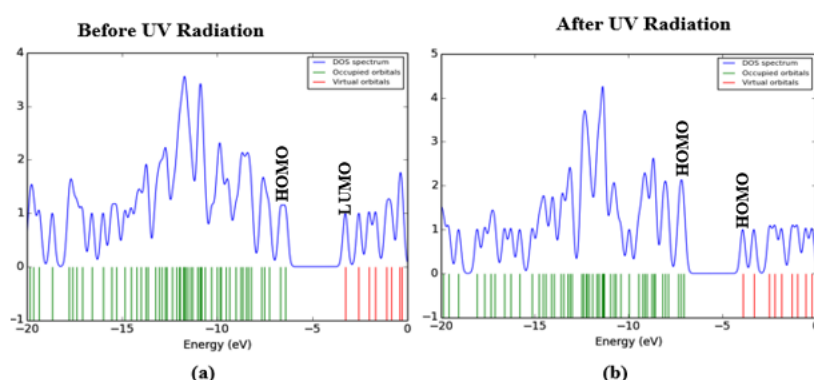


Figure 5. DOS charts form-CP (a) before, (b) after UV exposure.

3.5. Influence UV exposure on m-CP optical response.

Authors inspect UV exposure impact on m-CP physical features. Since m-CP holds over many terminal hydrogens (see Fig. 1), which can be decidedly influenced by UV radiation, authors speculate that UV photons attacked hydrogens associated with both OH groups promoting hydrogen proton splitting. Such an unexpected change raises the electron density around O atoms [38]. First, the lone pair of O₄₄ interact with contiguous C₅ form a π conjugation. Second, the other lone pair of O₃₃ remains free resonating through the whole SO₃ group. The UV exposure effect can be noticed from listed computed thermochemistry data (cf. Table 3). Irradiated m-CP dipole-moment has improved up to 8.99 D, and HOMO~LUMO offset has lowered to 2.66 eV. Such surprising influence on bandgap offset and dipole-moment will trigger an efficient electron rush process through FMOs. Consequently, irradiated m-CP

reserve primer position as outstanding window layer for solar cell applications [39-42]. Fig. 4-b presents calculated irradiated m-CP HOMO/LUMO offset while Fig. 5-b shows computed DOS chart for irradiated m-CP as well.

3.6. Polarizability/hyperpolarizability calculations.

Polarizabilities and 1st hyperpolarizabilities are computed to inspect NLO response for m-CP before and after UV exposure through WB97XD6-311G calculation level. Mean-polarizability [α_{tot}], polarizability anisotropy [$\Delta\alpha$] and 1st hyperpolarizability [β_{tot}] are computed by later mathematical formalism [43]:

$$\alpha_{tot} = \frac{1}{3} (\alpha_{xx} + \alpha_{yy} + \alpha_{zz})$$

$$\Delta\alpha = \sqrt{\frac{1}{2} ((\alpha_{xx} - \alpha_{yy})^2 + (\alpha_{yy} - \alpha_{zz})^2 + (\alpha_{zz} - \alpha_{xx})^2 + 6\alpha_{yz}^2 + 6\alpha_{xy}^2 + 6\alpha_{xz}^2)^{\frac{1}{2}}}$$

$$\beta_{tot} = \sqrt{(\beta_{xyy} + \beta_{xzz} + \beta_{xxx})^2 + (\beta_{yzz} + \beta_{yxx} + \beta_{yyy})^2 + (\beta_{zxx} + \beta_{zyy} + \beta_{zzz})^2}$$

Enhancement in material NLO response is related right away by how TDM, α_{tot} and β_{tot} values can be increased. The higher TDM, α_{tot} and β_{tot} values are, the better NLO response be. Table 5 shows 1st hyperpolarizability (β_{tot}), $\Delta\alpha$ and α_{tot} for m-CP before and after UV-exposure. The α_{tot} and $\Delta\alpha$ values for m-CP before and after UV exposure are $40.85*10^{-24}$, $22.69*10^{-24}$ and $40.25*10^{-24}$, $28.19*10^{-24}$ e.su, respectively. The β_{tot} for m-CP before and after UV-exposure are $11.53*10^{-30}$ and $1.87*10^{-30}$ e.su, respectively. M-CP NLO response has been lowered after UV-exposure, which may be explained by excitons formation inside irradiated m-CP. The 1st hyperpolarizability (β_{tot}) form-CP is 31 times above urea ($\beta_{urea} = 0.3728 *10^{-30}$ e.su). Such a magnificent NLO response nominates m-CP material as premier in NLO technologies.

Table 5. Mean-polarizability α_{tot} , polarizability anisotropy $\Delta\alpha$ and 1st hyperpolarizability β_{tot} for m-CP before and after UV exposure.

Parameters	Polarizability (*10 ⁻²⁴ e.su)		Hyperpolarizability (*10 ⁻³⁰ e.su)	
	Before UV	After UV	Before UV	After UV
α_{xx}	361.08	360.46	β_{xxx}	7.07
α_{xy}	-15.83	-0.08	β_{xyy}	5.40
α_{yy}	269.81	277.16	β_{yyz}	3.07
α_{xz}	-11.91	-7.96	β_{yyz}	0.91
α_{yz}	24.32	7.82	β_{xzz}	0.10
α_{zz}	196.10	177.17	β_{xyz}	-0.83
α_{tot}	40.85	40.25	β_{yzz}	0.09
$\Delta\alpha$	22.69	23.73	β_{xzz}	-0.28
			β_{yzz}	-0.40
			β_{zzz}	0.73
			β_{tot}	11.53
				1.87

3.7. ADME parameters and bioactivity.

Swiss-ADME for estimating physicochemical descriptors. Smile notation of the m-CP is Oc1ccc(c(c1)C)C1(OS(=O)(=O)c2c1cccc2)c1ccc(cc1C)O. m-CP's remarkable biological activity emerges from the hydroxytoluene ring plays a significant role in its antimicrobial activity. Bioavailability Radar (see Fig 6-a) demonstrates product similarity of m-CP. It is also used to anticipate characterizations like ADME, pharmacokinetics, therapeutic drug features, listed in Table 6. Six physicochemical characteristics of m-CP have been tested, namely

lipophilicity, size polarity, solubility, edibility, and saturation, which confirms that both isomers of m-CP are ingested through both respiratory/gastrointestinal systems and intact skin as well [44].

Table 6. Biological activity and ADME parameters of m-CP.

Physicochemical Properties		Water Solubility	
Formula	C ₂₁ H ₁₈ O ₅ S	Log S [ESOL]	-4.93
Molecular weight	382.43 g/mol	Solubility	4.44*10 ⁻³ mg ml ⁻¹ ; 1.16*10 ⁻⁵ mol/l
No. Non-H atoms	27	Class	Moderately soluble
No. Ar. Non-H atoms	18	Log S [Ali]	-5.38
Fractional Csp3	0.14	Solubility	1.60 *10 ⁻³ mg ml ⁻¹ ; 4.18 *10 ⁻⁶ mol/l
No. rotational bonds	2	Class	Mid solubility
No. H-bond acceptors	5	Log S [SILICOS-IT]	-6.92
No. H-bond donors	2	Solubility	4.61e*10 ⁻⁵ mg ml ⁻¹ ; 1.21*10 ⁻⁷ mol/l
Molar-Refractivity	101.50	Class	Poor solubility
TPSA	92.21 Å ²		
Lipophilicity		Drug-likeness	
Log [P _{o/w}] [iLOGP]	2.23	Lipinski	Y; 0 violation
Log [P _{o/w}] [XLOGP3]	3.75	Ghose	Y
Log [P _{o/w}] [WLOGP]	4.70	Veber	Y
Log [P _{o/w}] [MLOGP]	3.18	Egan	Y
Log [P _{o/w}] [SILICOS-IT]	3.82	Muegge	Y
Consensus Log [P _{o/w}]	3.54	Bioavailability Score	0.55
Pharmacokinetics		Medicinal Chemistry	
GI absorption	H	PAINS	1 alert: phenol_sulfite_A
BBB permeant	Nil	Brenk	1 alert: sulfonic_acid_1
P-gp substrate	Y	Lead likeness	No; 2 violations: MW > 350, XLOGP3 > 3.5
CYP1A2	Y	Synthetic accessibility	4.03
CYP2C19	N		
CYP2C9	N		
CYP2D6	N		
CYP3A4	N		
Log K _p (skin permeation)	-5.97 cm s ⁻¹		

Ar (Aromatic); Ali (Aliphatic); H(High); Y (Yes); N(No)

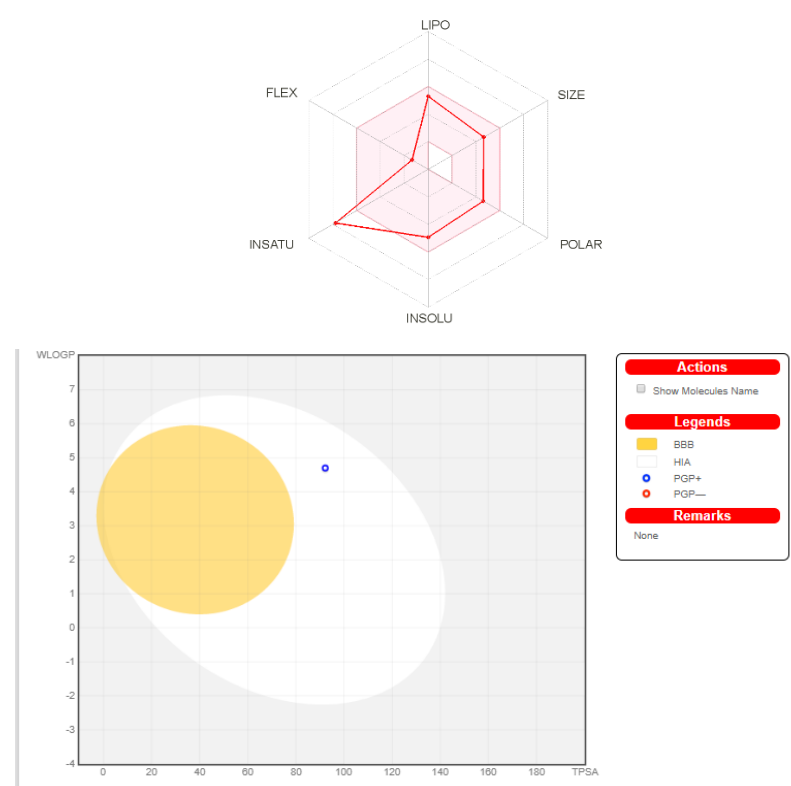


Figure 6. (a) ADME representation (b) Boiled-Egg predictive model for m-CP.

m-CP is reported to have a high absorption of Gastrointestinal (GI) in Pharmacokinetics. Definite results suggest that m-CP largely transmitted all cross body after uptake. m-CP usually mixes with inorganic sulfate and glucuronic acid, which excretes as urine agonists [45]. It has BBB zero, suggesting that they are strongly hydrophilic, polar chemicals to predict bowel permeation.

m-CP physicochemical spectrum adapted as a pink zone on each axis to be a well-defined descriptor of the drug, which yields a predictive model, Boiled-Egg (see Fig. 6-b). Molecules that are favorably absorbed by the gastrointestinal tract are presented as white space, while those who penetrate the brain are presented by yellow (yolk) one.

3.8. Pharmaco-kinetic properties and QSAR studies.

Bioactivity provides information on the qualitative assessment of physicochemical properties that make an oral drug molecule possible. The bioavailability of the title molecule is 55% as m-CP isomers are specifically used in bactericides or disinfectants as the active ingredient [46]. Both ρ -cresyl and ρ -cresyl sulfate, namely cresol metabolites, showed human protein/albumin binding ratio of approximately 13-20% [47]. Table 7 represents m-CP biological activity score. Target cases with protein binding percentages and molecular lipophilicity potential for Cresol molecule are shown in Fig. 7(a&b), which confirm that ligand interacts with the proposed nuclear reactor by 33%.

Table 7. Biological activity score for m-CP.

Target	Bioactivity score
GPCR-ligand	0.01
Ion-channel modulator	-0.20
Kinase-inhibitor	-0.10
Nuclear receptor-ligand	0.08

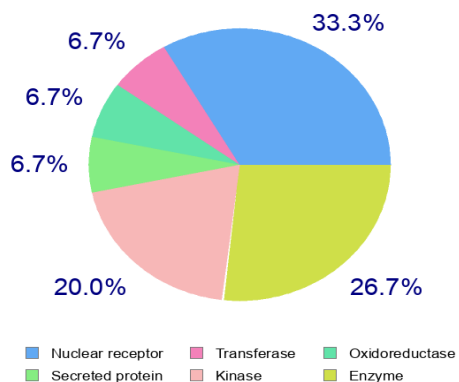


Figure 7. (a) Target cases with the percentage of protein binding for m-CP.

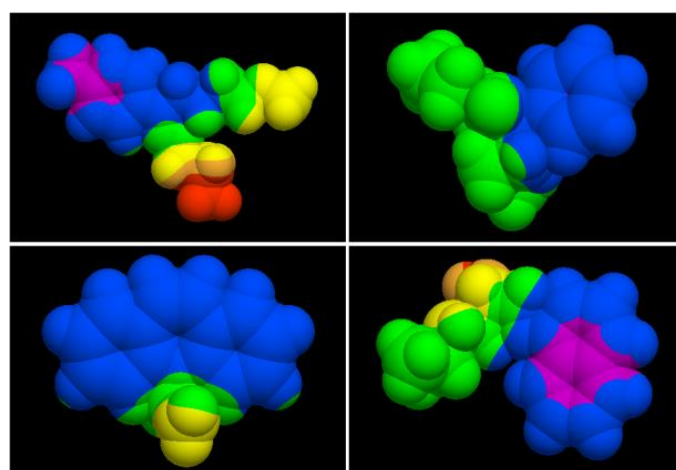


Figure 7. (b) Molecular lipophilicity potential of m-CP.

3.9. Micro species distribution and topological analysis.

Especially, pH distribution is a useful property for drug discovery, log D (pH) values for a series of compounds are used to calculate potential absorption sites from GI tract. Actually, pH is the most awaited drug discovery element. The typical logarithm of pH micro species presents with H bond donor and Cresol acceptor sites in range 0~14 is described in Fig. 8, and pH calculated results are listed in Table 8. Polar surface area (2D) of m-CP is 83.83A^2 , pH max is 7.40 and surface area (3D) of Van der Waals = 522.51A^2 . Refractivity of m-CP is $94.12 \text{ m}^3 \text{ mol}^{-1}$ Polarizability 34.9 \AA^3 , Number of Rings 4, pKa (high-acidic) (high-basic) are 9.16 and -6, respectively. Active sites that are charged negatively and positively are given both lower and higher local pH.

Table 8. pH values with donor and acceptor distribution of m-CP.

pH value	Donor	Acceptor
0.00	2.00	8.00
0.50	2.00	8.00
1.00	2.00	8.00
1.50	2.00	8.00
2.00	2.00	8.00
2.50	2.00	8.00
3.00	2.00	8.00
3.50	2.00	8.00
4.00	2.00	8.00
4.50	2.00	8.00
5.00	2.00	8.00
5.50	2.00	8.00
6.00	2.00	8.00
6.50	2.00	8.00
7.00	1.99	8.01
7.50	1.98	8.02
8.00	1.95	8.05
8.50	1.85	8.15
9.00	1.59	8.41
9.50	1.10	8.90
10.00	0.56	9.44
10.50	0.22	9.78
11.00	0.07	9.93
11.50	0.02	9.98
12.00	0.01	9.99
12.50	0.00	10.00
13.00	0.00	10.00
13.50	0.00	10.00
14.00	0.00	10.00

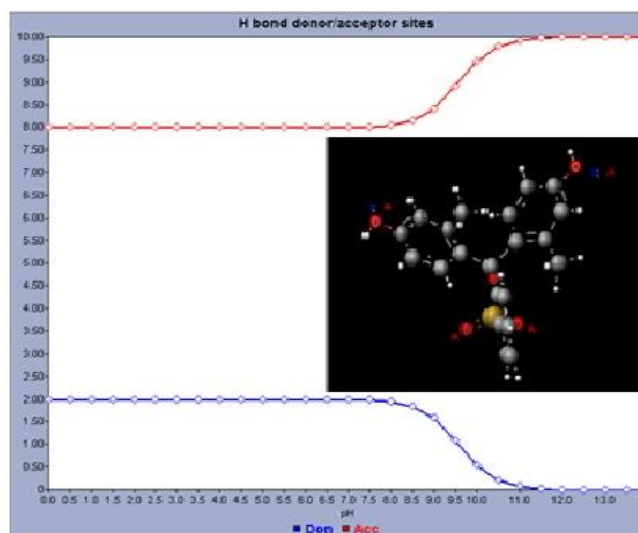


Figure 8. H bond donor/acceptor sites with pH values of m-CP.

Table 9 represents the Topological analysis of m-CP molecule. Phenol sulfonphthalein or m-CP is a pH sensor widely used in cell biology laboratories, or otherwise called phenol red. Due to its poor estrogenic compound's activity, phenol sulfonphthalein is being investigated for clinical application [48].

Table 9. Topological analysis of m-CP.

Count	Topological Analysis					
	Bond	Atom	Ring	Carbo-ring	Hetro	Fuse-ring
Total	48	45				
Aliphatic	12	9	1	0	1	0
Aromatic	18	18	3	3	0	0
Chain	8	6				
Ring	22	21				
Rotatory		2				
carbo			3			
Fused				2		
Hetero			1			

4. Conclusions

The theoretical research was performed m-CP, which exhibits outstanding electronic and photovoltaic properties and efficient drug-like behavior. A proper harmony between measured and predicted FTIR charts is observed. Single and double vibrational studies with predicted crystallographic data on m-CP dye have been reported. Unusual electrostatic interactions between O₃₃ and both C₂₂ and C₂₃ are observed to influence m-CP's NLO activity. FMO transitions and DOS Map promotes the manufacture of modern m-CP based solar devices and efficiencies. Both polarization and 1st hyperpolarization capabilities are measured to inspect NLO response for m-CP before and after exposure to UV using WB97XD6-311G level. In addition, m-CP obey Lipinski's law of five (RO5), which means that theoretically, such compounds should not have difficulties with oral dosage. ADME, pharmacokinetic properties, log P, pH value, biological activity, Boiled-Egg predictive model, QSAR, lipophilicity, microorganism distribution, target binding rate, and topological measurements are studied to aid with drug discovery. According to the authors' report bio-report, m-CP can be efficiently used as bactericides, pesticides, and disinfectants.

Funding

This research received no external funding.

Acknowledgments

This research has no acknowledgment.

Conflicts of Interest

The authors declare no conflict of interest.

References

- Irimia-Vladu, M.; Głowacki, E.D.; Troshin, P.A.; Schwabegger, G.; Leonat, L.; Susarova, D.K.; Krystal, O.; Ullah, M.; Kanbur, Y.; Bodea, M.A.; Razumov, V.F.; Sitter, H.; Bauer, S.; Sariciftci, N.S. Indigo - A Natural Pigment for High Performance Ambipolar Organic Field Effect Transistors and Circuits. *Advanced Materials* **2012**, 24, 375-380, <https://doi.org/10.1002/adma.201102619>.

2. Abdelwahab, A.B.; El-Sawy, E.R.; Kirsch, G. Iron powder and tin/tin chloride as new reducing agents of Meerwein arylation reaction with unexpected recycling to anilines. *Synthetic Communications* **2020**, *50*, 526-538, <https://doi.org/10.1080/00397911.2019.1704786>.
3. Jakkampudi, S.; Konda, S.; Arman, H.; Zhao, J.C.G. Diastereodivergent Synthesis of Bridged Tetrahydroisoquinoline Derivatives Catalyzed by Modularly Designed Organocatalysts. *Advanced Synthesis & Catalysis* **2020**, *362*, 2419-2426, <https://doi.org/10.1002/adsc.202000227>.
4. Elmorsy, M.R.; Su, R.; Abdel-Latif, E.; Badawy, S.A.; El-Shafei, A.; Fadda, A.A. New cyanoacetanilides based dyes as effective co-sensitizers for DSSCs sensitized with ruthenium (II) complex (HD-2). *Journal of Materials Science: Materials in Electronics* **2020**, *31*, 7981-7990, <https://doi.org/10.1007/s10854-020-03337-3>.
5. Asif, M.; Hassanain, M.A.; Nahiduzzaman, K.M.; Sawalha, H.J.E. Smart and Sustainable Built Environment. *Smart and Sustainable Built Environment* **2019**, *8*, 34-52, <https://doi.org/10.1108/SASBE-06-2018-0032>.
6. Dinparast, L.; Hemmati, S.; Alizadeh, A.A.; Zengin, G.; Kafil, H.S.; Bahadori, M.B.; Dastmalchi, S. An efficient, catalyst-free, one-pot synthesis of 4H-chromene derivatives and investigating their biological activities and mode of interactions using molecular docking studies. *Journal of Molecular Structure* **2020**, *1203*, <https://doi.org/10.1016/j.molstruc.2019.127426>.
7. Pešić, M.; Bugarinović, J.; Minić, A.; Novaković, S.B.; Bogdanović, G.A.; Todosijević, A.; Stevanović, D.; Damljanović, I. Electrochemical characterization and estimation of DNA-binding capacity of a series of novel ferrocene derivatives. *Bioelectrochemistry* **2020**, *132*, <https://doi.org/10.1016/j.bioelechem.2019.107412>.
8. Saji, R.S.; Prasana, J.C.; Muthu, S.; George, J.; Kuruvilla, T.K.; Raajaraman, B.R. Spectroscopic and quantum computational study on naproxen sodium. *Spectrochimica Acta Part A: Molecular and Biomolecular Spectroscopy* **2020**, *226*, <https://doi.org/10.1016/j.saa.2019.117614>.
9. El-Mansy, M. FT-IR, FT-Raman Spectra and Ab Initio HF, DFT Vibrational Analysis of P-methyl acetanilide. *Journal of Applied Sciences Research* **2009**, *5*, 1977-1987.
10. El-Mansy, M.A.M.; El-Nahass, M.M.; Khusayfan, N.M.; El-Menawy, E.M. DFT approach for FT-IR spectra and HOMO-LUMO energy gap for N-(p-dimethylaminobenzylidene)-p-nitroaniline (DBN). *Spectrochimica Acta Part A: Molecular and Biomolecular Spectroscopy* **2013**, *111*, 217-222, <https://doi.org/10.1016/j.saa.2013.04.018>.
11. El-Mansy, M.A.M.; Ismail, M.M. On the spectroscopic analyses of 3-(4-Hydroxy-1-methyl-2-oxo-1,2-dihydro-quinolin-3-yl)-2-nitro-3-oxo-propionic acid (HMQNP). *Spectrochimica Acta Part A: Molecular and Biomolecular Spectroscopy* **2015**, *135*, 704-709, <https://doi.org/10.1016/j.saa.2014.07.033>.
12. El-Mansy, M.A.M.; Yahia, I.S. Spectroscopic notes of Methyl Red (MR) dye. *Spectrochimica Acta Part A: Molecular and Biomolecular Spectroscopy* **2014**, *130*, 59-63, <https://doi.org/10.1016/j.saa.2014.03.113>.
13. El-Nahass, M.M.; Kamel, M.A.; El-Barbary, A.A.; El-Mansy, M.A.M.; Ibrahim, M. FT-IR spectroscopic analyses of 3-Methyl-5-Pyrazolone (MP). *Spectrochimica Acta Part A: Molecular and Biomolecular Spectroscopy* **2013**, *111*, 37-41, <https://doi.org/10.1016/j.saa.2013.03.072>.
14. Ibrahim, M.; El-Barbary, A.A.; El-Nahass, M.M.; Kamel, M.A.; El-Mansy, M.A.M.; Asiri, A.M. On the spectroscopic analyses of (E)-3-(dicyclopropyl methylene)-dihydro-4-[1-(2,5 dimethylfuran-3-yl) ethylidene]furan-2,5-dione. *Spectrochimica Acta Part A: Molecular and Biomolecular Spectroscopy* **2012**, *87*, 202-208, <https://doi.org/10.1016/j.saa.2011.11.039>.
15. Ibrahim, M.; El-Nahass, M.M.; Kamel, M.A.; El-Barbary, A.A.; Wagner, B.D.; El-Mansy, M.A.M. On the spectroscopic analyses of thioindigo dye. *Spectrochimica Acta Part A: Molecular and Biomolecular Spectroscopy* **2013**, *113*, 332-336, <https://doi.org/10.1016/j.saa.2013.05.014>.
16. Ismail, M.M.; Morsy, G.M.; Mohamed, H.M.; El-Mansy, M.A.M.; Abd-Alrazk, M.M.A. FT-IR spectroscopic analyses of 4-hydroxy-1-methyl-3-[2-nitro-2-oxoacetyl-2(1H)quinolinone (HMNOQ)]. *Spectrochimica Acta Part A: Molecular and Biomolecular Spectroscopy* **2013**, *113*, 191-195, <https://doi.org/10.1016/j.saa.2013.04.117>.
17. Soliman, H.S.; Eid, K.M.; Ali, H.A.M.; Atef, S.M.; El-Mansy, M.A.M. Vibrational spectroscopic analysis of 2-chloro-5-(2,5-dimethoxy-benzylidene)-1,3-diethyl-dihydro-pyrimidine-4,6(1H,5H)-dione. *Spectrochimica Acta Part A: Molecular and Biomolecular Spectroscopy* **2012**, *97*, 1079-1084, <https://doi.org/10.1016/j.saa.2012.07.104>.
18. Soliman, H.S.; Eid, K.M.; Ali, H.A.M.; El-Mansy, M.A.M.; Atef, S.M. FT-IR spectroscopic analyses of 2-(2-furanylmethylene) propanedinitrile. *Spectrochimica Acta Part A: Molecular and Biomolecular Spectroscopy* **2013**, *105*, 545-549, <https://doi.org/10.1016/j.saa.2012.12.051>.
19. Hassnin, H. Nucleophilic substitution and ring transformation reactions with 4-chloro-6-ethyl-3-nitropyran[3,2-c]quinoline-2,5(6H)-dione. *Arkivoc* **2012**, *2012*, 384-397, <http://dx.doi.org/10.3998/ark.5550190.0013.634>.
20. Frisch, M.J.; Schlegel, G.W.T.H.B.; Scuseria, G.E.; Robb, M.A.; Cheeseman, J.R.; Montgomery, Jr.J.A.; Vreven, T.; Kudin, K.N.; Burant, J.C.; Millam, J.M.; Iyengar, S.S.; Tomasi, J.; Barone, V.; Mennucci, B.; Cossi, M.; Scalmani, G.; Rega, N.; Petersson, G.A.; Nakatsuji, H.; Hada, M.; Ehara, M.; Toyota, K.; Fukuda, R.; Hasegawa, J.; Ishida, M.; Nakajima, T.; Honda, Y.; Kitao, O.; Nakai, H.; Klene, M.; Li, X.; Knox, J.E.;

- Hratchian, H.P.; Cross, J.B.; Adamo, C.; Jaramillo, J.; Gomperts, R.; Stratmann, R.E.; Yazyev, O.; Austin, A.J.; Cammi, R.; Pomelli, C.; Ochterski, J.W.; Ayala, P.Y.; Morokuma, K.; Voth, G.A.; Salvador, P.; Dannenberg, J.J.; Zakrzewski, V.G.; Dapprich, S.; Daniels, A.D.; Strain, M.C.; Farkas, O.; Malick, D.K.; Rabuck, A.D.; Raghavachari, K.; Foresman, J.B.; Ortiz, J.V.; Cui, Q.; Baboul, A.G.; Clifford, S.; Cioslowski, J.; Stefanov, B.B.; Liu, G.; Liashenko, A.; Piskorz, P.; Komaromi, I.; Martin, R.L.; Fox, D.J.; Keith, T.; Al-Laham, A.M.; Peng, C.Y.; Nanayakkara, A.; Challacombe, M.; Gill, P.M.W.; Johnson, B.; Chen, W.; Wong, M.W.; Gonzalez, C.; Pople, J.A. Inc., Wallingford CT **2009**.
21. Frisch, A.; Dennington, R.; Keith, T.; Millam, J.; Nielsen, A.; Holder, A.; Hiscocks, J. Gaussian Inc. Wallingford, CT, USA **2009**.
22. El-Mansy, M.A.M. Quantum chemical studies on structural, vibrational, nonlinear optical properties and chemical reactivity of indigo carmine dye. *Spectrochimica Acta Part A: Molecular and Biomolecular Spectroscopy* **2017**, *183*, 284-290, <https://doi.org/10.1016/j.saa.2017.04.047>.
23. Xiao, F.; Yao, S.; Wang, J.; Wei, J.; Amirkhanian, S. Physical and chemical properties of plasma treated crumb rubbers and high temperature characteristics of their rubberised asphalt binders. *Road Materials and Pavement Design* **2020**, *21*, 587-606, <https://doi.org/10.1080/14680629.2018.1507922>.
24. Chaudhary, J.P.; Kholiya, F.; Vadodariya, N.; Budheliya, V.M.; Gogda, A.; Meena, R. Carboxymethylagarose-based multifunctional hydrogel with super stretchable, self-healable having film and fiber forming properties. *Arabian Journal of Chemistry* **2020**, *13*, 1661-1668, <https://doi.org/10.1016/j.arabjc.2017.12.034>.
25. Sureshkumar, B.; Mary, Y.S.; Panicker, C.Y.; Suma, S.; Armaković, S.; Armaković, S.J.; Van Alsenoy, C.; Narayana, B.J.A.J.o.C. Quinoline derivatives as possible lead compounds for anti-malarial drugs: spectroscopic, DFT and MD study. *Arabian Journal of chemistry* **2020**, *13*, 632-648. <https://doi.org/10.1016/j.arabjc.2017.07.006>
26. Gulácsi, M.; El-Mansy, M.A.M.; Gulácsi, Z. Electron-phonon interactions in conducting polymers. *Philosophical Magazine Letters* **2016**, *96*, 67-75, <https://doi.org/10.1080/09500839.2016.1150611>.
27. Baú, J.P.T.; Anizelli, P.R.; de Santana, H.; da Costa, M.F.; Zaia, D.A.M. An experimental and theoretical vibrational study of the interaction of cytosine and uracil with artificial seawaters: A prebiotic chemistry experiment. *Vibrational Spectroscopy* **2019**, *101*, 92-99, <https://doi.org/10.1016/j.vibspec.2019.02.002>.
28. Salih, T.; Salih, H.A.J.A.-M.J.f.P.S. In Silico Design and Molecular Docking Studies of Carbapenem Analogues Targeting Acinetobacter baumannii PBP1A Receptor. *Iraq Academic Scientific Journals* **2020**, *20*.
29. Koepsell, H. Organic Cation Transporters in Health and Disease. *Pharmacol Rev* **2020**, *72*, 1-45. <https://doi.org/10.1124/pr.118.015578>.
30. Arrousse, N.; Salim, R.; Kaddouri, Y.; zarrouk, A.; Zahri, D.; Hajjaji, F.E.; Touzani, R.; Taleb, M.; Jodeh, S. The inhibition behavior of two pyrimidine-pyrazole derivatives against corrosion in hydrochloric solution: Experimental, surface analysis and in silico approach studies. *Arabian Journal of Chemistry* **2020**, *13*, 5949-5965, <https://doi.org/10.1016/j.arabjc.2020.04.030>.
31. Motamarri, P.; Das, S.; Rudraraju, S.; Ghosh, K.; Davydov, D.; Gavini, V. DFT-FE – A massively parallel adaptive finite-element code for large-scale density functional theory calculations. *Computer Physics Communications* **2020**, *246*, <https://doi.org/10.1016/j.cpc.2019.07.016>.
32. Lgaz, H.; Salghi, R.; Masroor, S.; Kim, S.-H.; Kwon, C.; Kim, S.Y.; Yang, Y.-J.; Chung, I.-M. Assessing corrosion inhibition characteristics of hydrazone derivatives on mild steel in HCl: Insights from electronic-scale DFT and atomic-scale molecular dynamics. *Journal of Molecular Liquids* **2020**, *308*, <https://doi.org/10.1016/j.molliq.2020.112998>.
33. Rajamani, P.; Vijayakumar, V.; Nagaraj, P.; Sundaraganesan, N. Synthesis, Characterization, Spectroscopic, DFT and Molecular Docking Studies of 3-(3,4-Dihydroxyphenyl)-1-Phenyl-3-(Phenylamino)Propan-1-One. *Polycyclic Aromatic Compounds* **2020**, *1*-21, <https://doi.org/10.1080/10406638.2020.1837190>.
34. Montoro, O.R.; Tortajada, J.; Lobato, Á.; Baonza, V.G.; Taravillo, M. Theoretical (DFT) and experimental (Raman and FTIR) spectroscopic study on communic acids, main components of fossil resins. *Spectrochimica Acta Part A: Molecular and Biomolecular Spectroscopy* **2020**, *224*, <https://doi.org/10.1016/j.saa.2019.117405>.
35. Zhang, C.; Cao, H.; Wang, C.; He, M.; Zhan, W.; Guo, Y. Catalytic mechanism and pathways of 1, 2-dichloropropane oxidation over LaMnO₃ perovskite: An experimental and DFT study. *Journal of Hazardous Materials* **2021**, *402*, <https://doi.org/10.1016/j.jhazmat.2020.123473>.
36. Yousefi, S.; Ansari, R.; Aghdasi, P.; Mozhavi, S.M. Structural and mechanical properties characterization of arsenene nanosheets under doping effect of transition metals: A DFT study. *Physica E: Low-dimensional Systems and Nanostructures* **2020**, *124*, <https://doi.org/10.1016/j.physe.2020.114349>.
37. Liu, A.; Liang, X.; Ren, X.; Guan, W.; Gao, M.; Yang, Y.; Yang, Q.; Gao, L.; Li, Y.; Ma, T. Recent Progress in MXene-Based Materials: Potential High-Performance Electrocatalysts. *Advanced Functional Materials* **2020**, *30*, <https://doi.org/10.1002/adfm.202003437>.

38. Hamioud, F.; Tariq, S.; Batool, A.; Mubarak, A.A. Theoretical investigation on orthorhombic XMnO₃ (X = Nd, Dy and Ho) perovskite manganates using DFT. *Chemical Physics Letters* **2020**, *760*, <https://doi.org/10.1016/j.cplett.2020.138005>.
39. Dutta, R.; Ahmed, S.; Kalita, D.J. Theoretical design of new triphenylamine based dyes for the fabrication of DSSCs: A DFT/TD-DFT study. *Materials Today Communications* **2020**, *22*, <https://doi.org/10.1016/j.mtcomm.2019.100731>.
40. El-Mansy, M.; Ismail, M. Structural, conformational, optical, and nonlinear optical behavior of ethyl (6-ethyl 5, 6-dihydro 4, 5-dioxo 4 H pyrano [3, 2-c] quinolin-3yl) 2-oxoacetate (EPQOA): comparative theoretical and experimental studies. *Optical Quantum Electronics* **2021**, *53*, <https://doi.org/10.1007/s11082-021-02749-7>.
41. El-Mansy, M.; Osman, W.; Abdelsalam, H. The electronic and optical absorption properties of pristine, homo and hetero Bi-nanoclusters. *Chemical Physics* **2021**, *111113*, <https://doi.org/10.1016/j.chemphys.2021.111113>.
42. Bayoumy, A.M.; Osman, Y.O.; Elhaes, H.; Ibrahim, M.A.; El-Mansy, M.A. Effect of substitutions on the electronic properties of acetylsalicylic acid. *Optical Quantum Electronics* **2021**, *53*, <https://doi.org/10.1007/s11082-020-02725-7>.
43. Yaqoob, M.; Gul, S.; Zubair, N.F.; Iqbal, J.; Iqbal, M.A. Theoretical calculation of selenium N-heterocyclic carbene compounds through DFT studies: Synthesis, characterization and biological potential. *Journal of Molecular Structure* **2020**, *1204*, <https://doi.org/10.1016/j.molstruc.2019.127462>.
44. Çakmak, E.; Özbaşır İşin, D. A theoretical evaluation on free radical scavenging activity of 3-styrylchromone derivatives: the DFT study. *Journal of Molecular Modeling* **2020**, *26*, *1-11*, <https://doi.org/10.1007/s00894-020-04368-7>.
45. Attar, T.; Messaoudi, B.; Benhadria, N.J.C.T. DFT Theoretical Study of Some Thiosemicarbazide Derivatives with Copper. *Chemistry and Chemical Technology* **2020**, *14*, *20-25*, <https://doi.org/10.23939/chcht14.01.020>.
46. Drauch, V.; Ibesich, C.; Vogl, C.; Hess, M.; Hess, C. In-vitro testing of bacteriostatic and bactericidal efficacy of commercial disinfectants against *Salmonella Infantis* reveals substantial differences between products and bacterial strains. *International Journal of Food Microbiology* **2020**, *328*, <https://doi.org/10.1016/j.ijfoodmicro.2020.108660>.
47. Naumovski, V.; Kimble, B.; Laurenti, D.; Nammi, S.; Norimoto, H.; Chan, K. Polysaccharide peptide (PSP) extract from *Coriolus versicolor* decreased Tmax of tamoxifen and maintained biochemical serum parameters, with no change in the metabolism of tamoxifen in the rat. *Research Square* **2020**, <https://doi.org/10.3390/medicines7060035>.
48. Luo, X.; Lim, L.-T. An inkjet-printed sulfonephthalein dye indicator array for volatile amine detection. *Journal of Food Science* **2020**, *85*, *442-454*, <https://doi.org/10.1111/1750-3841.15020>.